Optical study of the antiferromagnetic ordered state in electron-overdoped $Ca_{0.77}Nd_{0.23}FeAs_2$

Run Yang,[1] Bing Xu,[2] Yaomin Dai,[3] Wei Zhang,[1,4] Jinyun Liu,[1] Ziyang Qiu,[1] and Xianggang Qiu[1,5,*]

[1]*Beijing National Laboratory for Condensed Matter Physics, Institute of Physics, Chinese Academy of Sciences, P.O. Box 603, Beijing 100190, China*

[2]*Center for High Pressure Science and Technology Advanced Research, Beijing 100094, China*

[3]*Center for Integrated Nanotechnologies, Los Alamos National Laboratory, Los Alamos, New Mexico 87545, USA*

[4]*College of Physics, Optoelectronics and Energy & Collaborative Innovation Center of Suzhou Nano Science and Technology, Soochow University, Suzhou 215006, China*

[5]*Collaborative Innovation Center of Quantum Matter, Beijing 100084, China*

(Received 12 March 2016; revised manuscript received 5 May 2016; published 6 June 2016)

In $Ca_{1-x}R_xFeAs_2$ (R = rare earth), an antiferromagnetic (AFM) phase as well as a structural transition have been reported, even in the electron-overdoped regime. Here, we investigated the temperature-dependent in-plane optical spectroscopy of overdoped $Ca_{0.77}Nd_{0.23}FeAs_2$. Upon entering the AFM state, we found an abrupt reduction of low-frequency (500–2000 cm^{-1}) spectral weight in the optical conductivity. In sharp contrast to the parent compounds of the 122 system, where spin-density-wave gaps have been clearly observed in the AFM state, a gap signature is absent in $Ca_{0.77}Nd_{0.23}FeAs_2$. This may be a consequence of the poor nesting condition between the hole and electron pockets. However, a spectral weight analysis shows that the reduced spectral weight at low frequency is transferred to the high-frequency range ($\gtrsim$4000 cm^{-1}), pointing to a localization effect. These observations suggest that the AFM order in $Ca_{0.77}Nd_{0.23}FeAs_2$ is most likely to originate from a localized nature rather than Fermi-surface nesting.

DOI: 10.1103/PhysRevB.93.245110

I. INTRODUCTION

Since unconventional superconductivity usually arises as a consequence of suppressing an antiferromagnetic (AFM) order in the parent compounds by chemical substitution, its pairing mechanism is believed to be intimately related to magnetism [1]. Understanding the origin of magnetism may provide an important clue to the unconventional pairing. The parent compounds of iron-based superconductors (FeSCs), such as $BaFe_2As_2$ [2] and LaFeAsO [3], generally feature well nested hole/electron pockets that undergo an AFM transition at low temperatures [4]. Charge doping can degrade the nesting condition to suppress the AFM transition, thus inducing superconductivity at the boundary of the AFM phase. Therefore, the pairing mechanism has been proposed to be associated with the scattering between the hole and electron pockets, which is induced by nesting-related spin-density-wave- (SDW-) type fluctuations [4,5]. In this picture, magnetism, as well as superconductivity, may strongly depend on the topology of the Fermi surface [6].

However, in FeTe, Fermi-surface nesting fails to account for the bicollinear AFM order [7]. Moreover, in $K_2Fe_4Se_5$ [8] and $(Li_{0.8}Fe_{0.2})$(OH)FeSe [9], even though no hole pockets exist at the Γ point, superconducting gaps still open on the Fermi surfaces. Thus, the pairing mechanism cannot be understood in terms of a Fermi-surface instability, and the electrons below the Fermi surface may also play an important role [4]. Moreover, Iimura *et al.* [10,11] have found another superconducting dome and AFM ordered state in an electron-overdoped area of $RFeAsO_{1-x}H_x$ (R = rare earth); these anomalous behaviors introduce additional puzzles and could reveal more rich physics in FeSCs. However, owing to the lack of a large sized single crystal, there is difficulty in carrying out detailed experiments.

$Ca_{1-x}R_xFeAs_2$ is a newly discovered iron-pnictide family with a monotonic structure (space group P_{21}) [12]. It consists of alternatively stacked FeAs and (Ca,R)As layers. Rare-earth doping on the Ca site can introduce electrons into the FeAs layers and induce superconductivity with $T_c = 35$ K ($x = 0.15$) [13]. With further electron doping, superconductivity is suppressed, however, instead of the Fermi-liquid (FL) behavior observed in some other iron pnictides, there is a recovery of the AFM order, which is confirmed by recent nuclear magnetic resonance (NMR) [14] and neutron scattering results [15], similar to what happened in $RFeAsO_{1-x}H_x$ [10]. Since the AFM is intimately related to superconductivity, studying such anomalous behavior may provide some new physics and shed light on the mechanism of unconventional superconductivity in FeSCs.

In this paper, we have synthesized single crystals of electron-overdoped $Ca_{0.77}Nd_{0.23}FeAs_2$ [12] ($T_N \lesssim 73$ K), and measured its temperature-dependent in-plane reflectivity before and after the AFM phase transition. To analyze the optical conductivity, we use two Drude components to describe the low-energy (<2000 cm^{-1}) response, to account for the multi-band nature of FeSCs [16,17]. Such a two-Drude model reveals a narrow temperature-dependent Drude item representing the coherent response, and a broad temperature-independent Drude one representing the incoherent response. Across the phase transition, we notice that the broad Drude component is significantly suppressed. Correspondingly, the spectral weight of optical conductivity at low frequency (50–2000 cm^{-1}) is reduced. Unlike the parent compound of the 122 system, the lack of a signature of a SDW transition in the optical conductivity indicates a poor nesting condition. However, a spectral weight analysis shows that the reduced spectral weight at low frequency is transferred to a high-frequency

*xgqiu@iphy.ac.cn

area ($\gtrsim$4000 cm^{-1}), indicating a localization effect, such as Hund's rule coupling. We infer that the magnetism in such an electron-overdoped system may come from a localization effect and does not rely on the topology of the Fermi surface.

II. EXPERIMENT

High-quality single crystals of $Ca_{1-x}Nd_xFeAs_2$ were synthesized by heating a mixture of Ca, Nd, FeAs, and As powders with a nominal composition of $x = 0.2$ [12,18], whose typical size was about $3 \times 3 \times 0.1$ mm^3. The composition determined by an inductively coupled plasma emission spectrometer (ICP) was $Ca_{0.77}Nd_{0.23}FeAs_2$. Resistivity measurements were taken on a Quantum Design physical property measurement system (PPMS). Magnetization was measured using a Quantum Design superconducting quantum interference device (SQUID). The reflectivity from the cleaved surface has been measured at a near-normal angle of incidence on a Fourier transform infrared spectrometer (Bruker 80v) for light polarized in the *ab* planes using an *in situ* evaporation technique [19]. Data from 40 to 15 000 cm^{-1} were collected at eight different temperatures from 15 to 300 K on an ARS-Helitran cryostat. The reflectivity in the visible and UV range (10 000–40 000 cm^{-1}) at room temperature was taken with an Avaspec 2048 $\times$ 14 optical fiber spectrometer. The optical conductivity has been determined from a Kramers-Kronig analysis of reflectivity $R(\omega)$ over the entire frequency range. Since the measurement is made in a limited energy range, a Hagen-Rubens relation ($R = 1 - A\sqrt{\omega}$) is used for low-frequency extrapolations. Above the highest measured frequency (40 000 cm^{-1}), $R(\omega)$ is assumed to be constant up to 40 eV, above which a free-electron response (ω^{-4}) is used [20].

III. RESULTS AND DISCUSSION

Figure 1(a) shows the temperature-dependent resistance with the $I \parallel ab$ plane and $I \parallel c$ axis. We note that above 73 K the in-plane resistance shows a metallic behavior which decreases upon cooling, while the interplane resistance shows an insulating behavior, i.e., it increases with decreasing temperature. It means that even though the CaAs layer has been reported to be metallic, the interlayer coupling is still weak. At 73 K, we note a sudden drop on both curves, and a kink could also be observed in its magnetic susceptibility [Fig. 1(b)]. These anomalies have been demonstrated to be caused by structural and AFM phase transitions [15]. Below 10 K, another drop in $R(T)$ [Fig. 1(a)] may come from filamentary superconductivity. In addition to these observations, we also note that, in the normal state, the in-plane resistance shows an obvious non-Fermi-liquid (NFL) behavior (discrepancy of the T^2 behavior) [17,21], but after the phase transition, the system becomes much more coherent. Such a phenomenon can be understood in terms of spin-fluctuation scattering, i.e., in the normal state, there exists strong spin fluctuation to scatter the carrier that results in NFL behavior, while in the magnetic ordered state the fluctuation is greatly suppressed [17].

The measured in-plane reflectivity and the real part of the optical conductivity $\sigma_1(\omega,T)$ are summarized in Fig. 2, for selected temperatures above and below the AFM phase

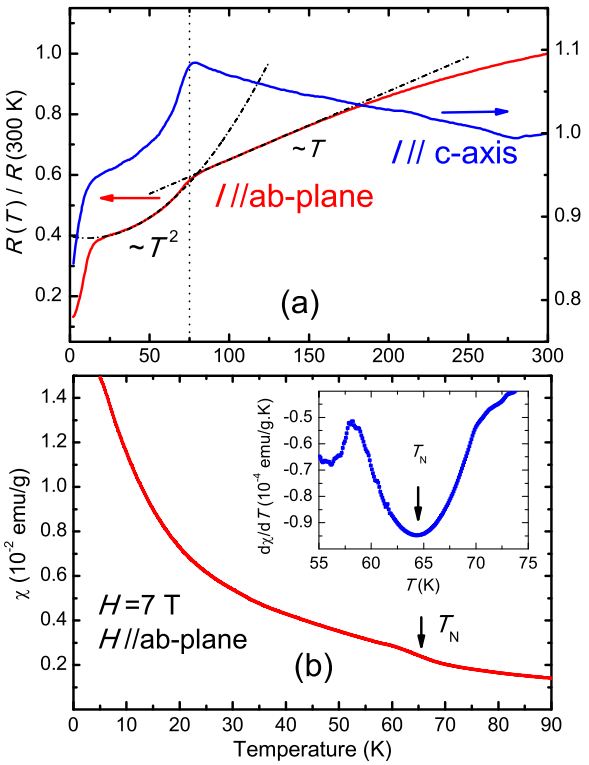

FIG. 1. (a) Temperature dependence of normalized resistivity of $Ca_{0.77}Nd_{0.23}FeAs_2$ with $I \parallel c$ axis (blue) and $I \parallel ab$ plane (red). (b) The temperature dependence of magnetic susceptibility of $Ca_{0.77}Nd_{0.23}FeAs_2$ with $H \parallel ab$ plane at 1 T. The inset is its derivative with temperature. Arrows indicate the Néel temperature.

transition. The reflectivity shows a typical metallic behavior, approaching unity at low frequencies (<1000 cm^{-1}) and increasing upon cooling. After the AFM phase transition, a suppression of $R(\omega,T)$ in the midinfrared range (500–2000 cm^{-1}) can be seen. Correspondingly, similar behavior is also found in the optical conductivity spectra, indicating a change in the band structure and a loss of density of states near the Fermi level. Compared with $BaFe_2As_2$, which also undergoes an AFM phase transition [22], below 73 K, no additional gaplike feature below 3000 cm^{-1} can be found, indicating no SDW transition occurred in $Ca_{0.77}Nd_{0.23}FeAs_2$—the reason for this will be discussed later.

To quantitatively analyze the optical data of $Ca_{0.77}Nd_{0.23}FeAs_2$, we fit the $\sigma_1(\omega,T)$ with a simple Drude-Lorentz mode for the dielectric function,

$$\epsilon(\omega) = \epsilon_\infty - \sum_i \frac{\Omega_{p,i}^2}{\omega^2 + \frac{i\omega}{\tau_i}} + \sum_j \frac{\Omega_j^2}{\omega_j^2 - \omega^2 - \frac{i\omega}{\tau_i}}, \quad (1)$$

where ϵ_∞ is the real part of the dielectric function at high frequencies, and the second term corresponds to the Drude response characterized by a plasma frequency $\Omega_{p,i}^2 = 4\pi ne^2/m^*$, with n a carrier concentration and m^* an effective mass, and $1/\tau_i$ the scattering rate. The third term is a sum of Lorentz oscillators characterized by a resonance frequency ω_j, a linewidth γ_j, and an oscillator strength Ω_j. The Drude term accounts for the itinerant carrier (intraband) response,

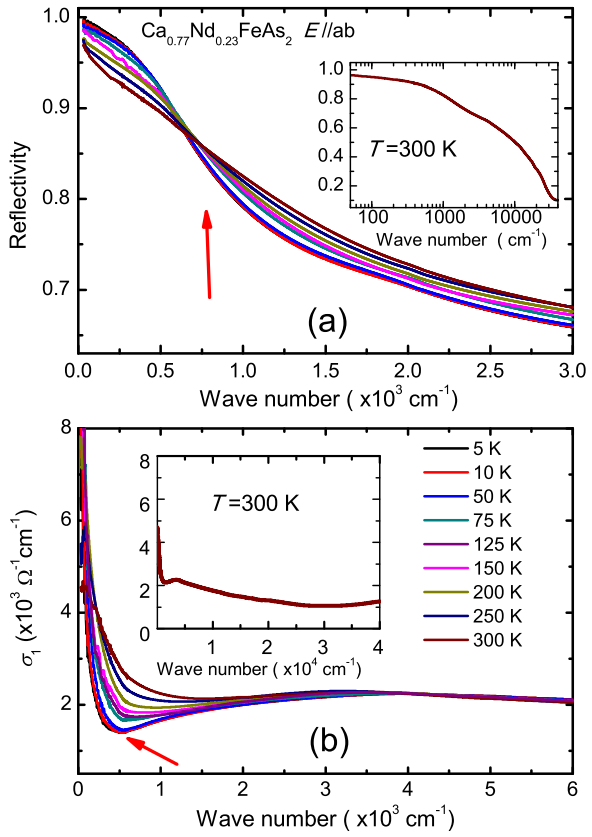

FIG. 2. (a) Reflectivity and (b) optical conductivity of $Ca_{0.77}Nd_{0.23}FeAs_2$ at various temperatures. The red arrows indicates the suppression in reflectivity and optical conductivity.

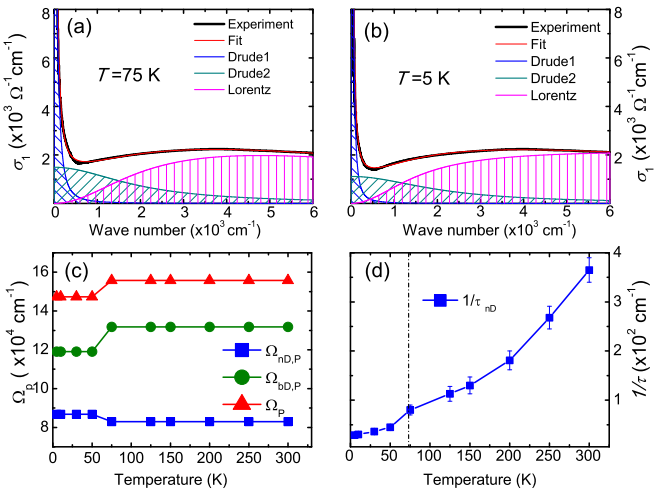

FIG. 3. (a), (b) Optical conductivity of $Ca_{0.77}Nd_{0.23}FeAs_2$ at 75 and 5 K (thick black lines), fitting with the Drude-Lorentz model (thin red lines), and its decomposition into individual Drude and Lorentz terms. (c) Plasma frequency for the narrow Drude (blue), broad Drude (green), and the total weights of the narrow and broad Drude components (red) for various temperatures. (d) T dependence of the quasiparticle scattering rate $1/\tau_{nD}$ derived from the coherent narrow Drude component. (The vertical dashed line denotes the phase transition.)

while the Lorentz contributions represent the localized (interband) excitations [23]. The complex conductivity $\tilde{\sigma}(\omega) = \sigma_1 + i\sigma_2 = i\omega[\tilde{\varepsilon}(\omega) - \varepsilon_\infty]/60$ (in units of $\Omega^{-1}\,\mathrm{cm}^{-1}$). The fitting results shown in Figs. 3(a) and 3(b) can well reproduce the experimental results.

Figures 3(a) and 3(b) summarize the fitting results, and considering the multiband nature of FeSCs, we use two Drude components (a narrow one and a broad one) and a Lorentz component to describe the optical response below 6000 cm^{-1}[16]. The narrow Drude item has a strongly temperature-dependent scattering rate at low temperature ($1/\tau_{nD} \simeq 32\ \mathrm{cm}^{-1}$, 10 K) and represents the coherent response. The scattering rate of the broad Drude item is 2000 cm^{-1} or larger, corresponding to a mean free path that is shorter than the lattice spacing and indicating a highly incoherent character [24,25]. The broad Drude item is much stronger than the narrow one, but it almost does not change with the temperature, representing an incoherent background [23]. Across the AFM transition, in Fig. 3(c) we note the broad Drude component is greatly suppressed. Meanwhile, the scattering rate of the coherent response is also reduced [Fig. 3(d)]. Considering the suppressed spin fluctuation in the AFM ordered state, we infer the incoherent response may have a relation with the AFM fluctuation. The overall plasma frequency Ω_p is considered to contribute from both narrow and broad Drude components with $\Omega_p = (\Omega_{nD,p}^2 + \Omega_{bD,p}^2)^{1/2}$. In Fig. 3(c), we note that even though the narrow Drude component is a little enhanced, the overall frequency is suppressed across the phase transition, indicating a loss of itinerant carriers after the transition. So where do the lost carriers go?

In Fig. 4(b), we have calculated the spectral weight in different areas of optical conductivity. From the results, one notes that the spectral weight at high energy (4000–15 000 cm^{-1}) varies significantly with the temperature. Upon cooling, the spectral weight at high frequency is continuously enhanced while the overall spectral weight keeps constant. It means the spectral weight at low frequency is transferred from a low- to high-frequency area. Such a pseudogaplike behavior has been widely attributed to the Hund's rule coupling effect, which can localize and polarize the itinerant electrons to enhance the electron correlation and AFM exchange interaction [26]. At low temperatures ($\lesssim$73 K), we observed an additional enhancement of the high-frequency spectral weight, and, combined with the result of the fitting analysis, we find that the suppressed spectral weight at the low-frequency area (500–2000 cm^{-1}) in the magnetic ordered state has been moved to the high-frequency area, reflecting a suddenly enhanced localization effect. Further research is needed to determine whether this effect is caused by Hund's rule coupling or some other effects.

Even though the spectral weight at the low-frequency area is greatly transferred to the high-frequency area during the phase transition, we do not observe any additional gaplike feature in the optical conductivity [Fig. 2(b)] after the AFM phase transition (evidence given by the spectral analysis is shown in Appendix B). This is different from what happened in $BaFe_2As_2$, which undergoes an SDW transition and has a signature of opening a gap in its optical spectrum [22].

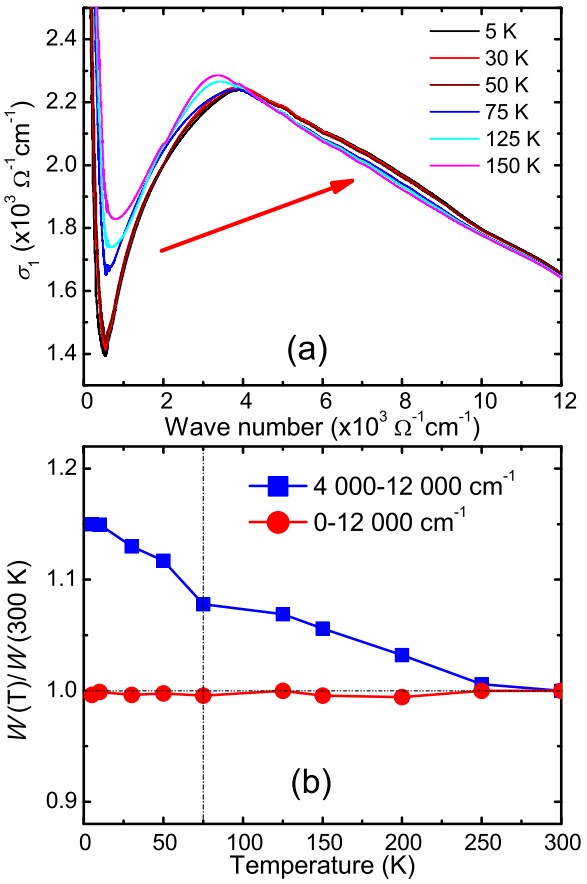

FIG. 4. (a) Enlarged optical conductivity of $Ca_{0.77}Nd_{0.23}FeAs_2$ before and after the phase transition, from which we could clearly see the spectral weight transference, indicated by the red arrow. (b) Temperature dependence of the spectral weight $W_{\omega_a}^{\omega_b} = \int_{\omega_a}^{\omega_b} \sigma_1(\omega) d\omega$ between different lower and upper cutoff frequencies. The vertical dashed line denotes the phase transition.

Comparing their Fermi surface, we note that $BaFe_2As_2$ as a compensate metal has equal sized electron and hole pockets, and there is good nesting between them along the (π,π) direction in the Brillouin zone [2,27]. This will lead to the instability of the Fermi surface and SDW transition at low temperatures [28]. Recent angle-resolved photoemission spectroscopy (ARPES) results on $Ca_{0.73}La_{0.27}FeAs_2$ indicate electron-overdoped FeAs layers [15], in which the electron pockets are much bigger than the hole pockets and lead to a poor nesting condition (compared with the less doped ones) and to no SDW transition and no gap on its Fermi surface. The AFM transition in such a poorly nested system suggests the magnetism in electron-overdoped $Ca_{0.77}Nd_{0.23}FeAs_2$ does not rely on the topology of the Fermi surface. The spectral weight transfer without a SDW gap creates a pseudogap feature in the optical spectrum across the AFM phase transition.

Such strong magnetism in electron-overdoped $Ca_{1-x}R_xFeAs_2$ cannot be understood by previous theoretical models [29,30], in which the electron doping could continuously suppress the magnetic order and low-energy spin fluctuation with worsening nesting conditions. Moreover, recent NMR results point out that magnetism is rather enhanced with doping [14], and such behavior cannot be understood in terms of the Fermi-surface nesting. Thus, the mechanism for magnetism in an overdoped area should be reconsidered.

Very recently, x-ray diffraction (XRD) experiments [15] on $Ca_{1-x}La_xFeAs_2$ found that the height of the As atom (in FeAs layer) corresponding to the Fe layer in an electron-overdoped sample ($x = 0.27$) is 1.422(5) Å, while it is 1.412(5) Å for the less doped one ($x = 0.195$) [12], indicating that rare-earth doping could somehow increase the pnictogen height in $Ca_{1-x}La_xFeAs_2$. Such behavior could enlarge the distance between the Fe and As atoms and suppress the hybridization between Fe $3d$ and As $4p$ orbitals [31]. As a result, electrons on Fe atoms could be much more localized, and the electron correlation as well as the local magnetic moment are enhanced [31,32]. Furthermore, across the AFM phase transition in $Ca_{0.73}La_{0.27}FeAs_2$, the lattice parameters a,b,c as well as the cell volume are found to be enlarged abruptly, and such a negative thermal expansion could narrow the bandwidth and localize the electrons, which is consistent with our observations in optical spectroscopy. Thus we propose that the magnetic transition is mostly like to have a localized origin. Even though an enhanced localization effect is accompanied with a phase transition, the system is still in a metallic state. From the fitting analysis of the optical data in Figs. 3(a) and 3(b), we note that the AFM transition mainly affects the broad Drude item, while the narrow one is almost unaffected. This may reflect the multiband nature of FeSCs [33,34], from which the much incoherent bands (or orbitals) are selected to be localized across the phase transition [35].

IV. SUMMARY

In summary, we have synthesized a single crystal of $Ca_{0.77}Nd_{0.23}FeAs_2$ and investigated its optical response at temperatures before and after the phase transition. From the optical conductivity, we find an obvious spectral weight transfer from the low- to high-energy area without any signature of a SDW gap across the AFM phase transition. Therefore, we propose the magnetism in electron-overdoped $Ca_{1-x}R_xFeAs_2$ may come from the localization effect, which results in a pseudogap feature, and does not rely on the Fermi-surface nesting. Since further electron doping by Co in $Ca_{0.73}La_{0.27}Fe_{1-x}Co_xAs_2$ could induce another superconducting dome [36], more investigations on this system may shed light on the mechanism of high-T_c superconductivity in FeSCs.

ACKNOWLEDGMENTS

We thank Kui Jin, Shiliang Li, Congcong Le, and Xianxin Wu for useful discussions. This work was supported by the NSFC MOST (973 Projects No. 2015CB921303, No. 2015CB921102, No. 2012CB921302, and No. 2012CB821403), and NSFC (Grants No. 91121004, No. 91421304, and No. 11374345).

APPENDIX A: HALL COEFFICIENT

To determine the electron concentration of $Ca_{0.77}Nd_{0.23}FeAs_2$, we measured its Hall resistance ρ_{xy} and

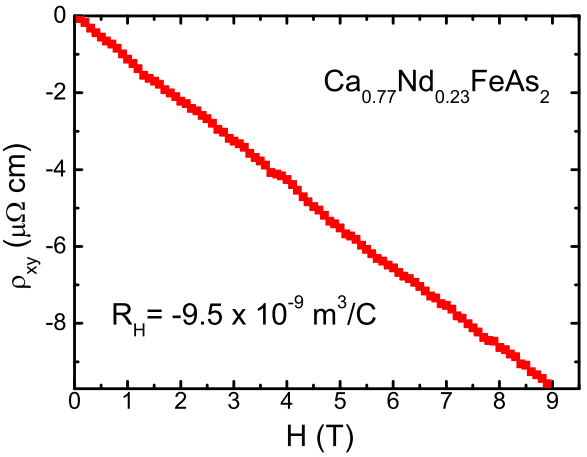

FIG. 5. Hall resistance and Hall coefficient of $Ca_{0.77}Nd_{0.23}FeAs_2$ at 300 K.

calculated the Hall coefficient at 300 K. The Hall coefficient of $Ca_{0.77}Nd_{0.23}FeAs_2$ at 300 K is -9.5×10^{-9} m^3/C, which is comparable with that of $Ca_{0.73}La_{0.27}FeAs_2$ [36], indicating that the $Ca_{0.77}Nd_{0.23}FeAs_2$ is electron overdoped. (See Fig. 5.)

APPENDIX B: DETAIL SPECTRAL WEIGHT ANALYSIS

In Fig. 6 we calculated the ratio of the spectral weight as a function of cutoff frequency for $BaFe_2As_2$ and $Ca_{0.77}Nd_{0.23}FeAs_2$, respectively. Comparing with $BaFe_2As_2$, we find no obvious signature characteristic of opening a gap within the SDW scale of $BaFe_2As_2$ but an enhanced spectral

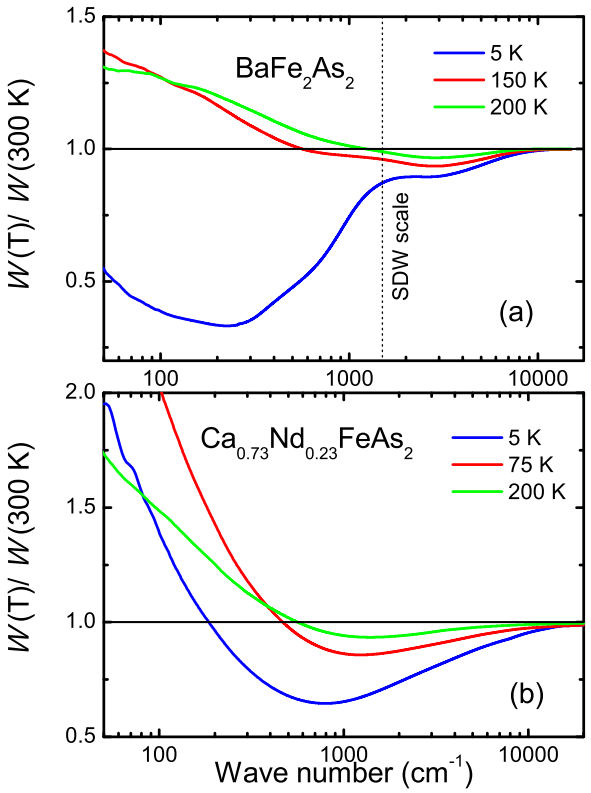

FIG. 6. Ratio of the integrated spectral weight $W(T)/W(300)$ as a function of cutoff frequency (wave number) in (a) $BaFe_2As_2$ and (b) $Ca_{0.77}Nd_{0.23}FeAs_2$.

weight transfer from a low- to high-energy area [Figs. 4(a) and 4(b)]. Such behavior might be regarded as pseudogap behavior.

[1] P. A. Lee, N. Nagaosa, and X.-G. Wen, Rev. Mod. Phys. **78**, 17 (2006).

[2] P. Richard, K. Nakayama, T. Sato, M. Neupane, Y.-M. Xu, J. H. Bowen, G. F. Chen, J. L. Luo, N. L. Wang, X. Dai, Z. Fang, H. Ding, and T. Takahashi, Phys. Rev. Lett. **104**, 137001 (2010).

[3] T. Yildirim, Phys. Rev. Lett. **101**, 057010 (2008).

[4] X. Chen, P. Dai, D. Feng, T. Xiang, and F.-C. Zhang, Nat. Sci. Rev. **1**, 371 (2014).

[5] I. I. Mazin, D. J. Singh, M. D. Johannes, and M. H. Du, Phys. Rev. Lett. **101**, 057003 (2008).

[6] Z. P. Yin, K. Haule, and G. Kotliar, Nat. Mater. **10**, 932 (2011).

[7] S. Li, C. de la Cruz, Q. Huang, Y. Chen, J. W. Lynn, J. Hu, Y.-L. Huang, F.-C. Hsu, K.-W. Yeh, M.-K. Wu, and P. Dai, Phys. Rev. B **79**, 054503 (2009).

[8] D.-x. Mou, L. Zhao, and X.-j. Zhou, Front. Phys. **6**, 410 (2011).

[9] L. Zhao, A. Liang, D. Yuan, Y. Hu, D. Liu, J. Huang, S. He, B. Shen, Y. Xu, X. Liu, L. Yu, G. Liu, H. Zhou, Y. Huang, X. Dong, F. Zhou, K. Liu, Z. Lu, Z. Zhao, C. Chen, Z. Xu, and X. J. Zhou, Nat. Commun. **7**, 10608 (2016).

[10] M. Hiraishi, S. Iimura, K. M. Kojima, J. Yamaura, H. Hiraka, K. Ikeda, P. Miao, Y. Ishikawa, S. Torii, M. Miyazaki, I. Yamauchi, A. Koda, K. Ishii, M. Yoshida, J. Mizuki, R. Kadono, R. Kumai, T. Kamiyama, T. Otomo, Y. Murakami, S. Matsuishi, and H. Hosono, Nat. Phys. **10**, 300 (2014).

[11] S. Iimura, S. Matuishi, H. Sato, T. Hanna, Y. Muraba, S. W. Kim, J. E. Kim, M. Takata, and H. Hosono, Nat. Commun. **3**, 943 (2012).

[12] N. Katayama, K. Kudo, S. Onari, T. Mizukami, K. Sugawara, Y. Sugiyama, Y. Kitahama, K. Iba, K. Fujimura, N. Nishimoto, M. Nohara, and H. Sawa, J. Phys. Soc. Jpn. **82**, 123702 (2013).

[13] M. Y. Li, Z. T. Liu, W. Zhou, H. F. Yang, D. W. Shen, W. Li, J. Jiang, X. H. Niu, B. P. Xie, Y. Sun, C. C. Fan, Q. Yao, J. S. Liu, Z. X. Shi, and X. M. Xie, Phys. Rev. B **91**, 045112 (2015).

[14] S. Kawasaki, T. Mabuchi, S. Maeda, T. Adachi, T. Mizukami, K. Kudo, M. Nohara, and G.-q. Zheng, Phys. Rev. B **92**, 180508 (2015).

[15] S. Jiang, C. Liu, H. Cao, T. Birol, J. M. Allred, W. Tian, L. Liu, K. Cho, M. J. Krogstad, J. Ma, K. M. Taddei, M. A. Tanatar, M. Hoesch, R. Prozorov, S. Rosenkranz, Y. J. Uemura, G. Kotliar, and N. Ni, Phys. Rev. B **93**, 054522 (2016).

[16] D. Wu, N. Barišić, P. Kallina, A. Faridian, B. Gorshunov, N. Drichko, L. J. Li, X. Lin, G. H. Cao, Z. A. Xu, N. L. Wang, and M. Dressel, Phys. Rev. B **81**, 100512 (2010).

[17] Y. M. Dai, H. Miao, L. Y. Xing, X. C. Wang, P. S. Wang, H. Xiao, T. Qian, P. Richard, X. G. Qiu, W. Yu, C. Q. Jin, Z. Wang, P. D. Johnson, C. C. Homes, and H. Ding, Phys. Rev. X **5**, 031035 (2015).
[18] K. Kudo, Y. Kitahama, K. Fujimura, T. Mizukami, H. Ota, and M. Nohara, J. Phys. Soc. Jpn. **83**, 093705 (2014).
[19] C. C. Homes, M. Reedyk, D. A. Cradles, and T. Timusk, Appl. Opt. **32**, 2976 (1993).
[20] Y. M. Dai, B. Xu, B. Shen, H. Xiao, H. H. Wen, X. G. Qiu, C. C. Homes, and R. P. S. M. Lobo, Phys. Rev. Lett. **111**, 117001 (2013).
[21] J. G. Analytis, H.-H. Kuo, R. D. McDonald, M. Wartenbe, P. M. C. Rourke, N. E. Hussey, and I. R. Fisher, Nat. Phys. **10**, 194 (2014).
[22] W. Z. Hu, J. Dong, G. Li, Z. Li, P. Zheng, G. F. Chen, J. L. Luo, and N. L. Wang, Phys. Rev. Lett. **101**, 257005 (2008).
[23] C. C. Homes, Y. M. Dai, J. S. Wen, Z. J. Xu, and G. D. Gu, Phys. Rev. B **91**, 144503 (2015).
[24] M. Nakajima, S. Ishida, T. Tanaka, K. Kihou, Y. Tomioka, T. Saito, C.-H. Lee, H. Fukazawa, Y. Kohori, T. Kakeshita, A. Iyo, T. Ito, H. Eisaki, and S.-i. Uchida, J. Phys. Soc. Jpn. **83**, 104703 (2014).
[25] M. Nakajima, S. Ishida, T. Tanaka, K. Kihou, Y. Tomioka, T. Saito, C. H. Lee, H. Fukazawa, Y. Kohori, T. Kakeshita, A. Iyo, T. Ito, H. Eisaki, and S. Uchida, Sci. Rep. **4**, 5873 (2014).
[26] N. L. Wang, W. Z. Hu, Z. G. Chen, R. H. Yuan, G. Li, G. F. Chen, and T. Xiang, J. Phys.: Condens. Matter **24**, 294202 (2012).
[27] P. Richard, T. Sato, K. Nakayama, T. Takahashi, and H. Ding, Rep. Prog. Phys. **74**, 124512 (2011).
[28] J. N. Hancock, S. I. Mirzaei, J. Gillett, S. E. Sebastian, J. Teyssier, R. Viennois, E. Giannini, and D. van der Marel, Phys. Rev. B **82**, 014523 (2010).
[29] P. Dai, J. Hu, and E. Dagotto, Nat. Phys. **8**, 709 (2012).
[30] H. Ikeda, R. Arita, and J. Kuneš, Phys. Rev. B **82**, 024508 (2010).
[31] J. Diehl, S. Backes, D. Guterding, H. O. Jeschke, and R. Valentí, Phys. Rev. B **90**, 085110 (2014).
[32] C. Zhang, L. W. Harriger, Z. Yin, W. Lv, M. Wang, G. Tan, Y. Song, D. L. Abernathy, W. Tian, T. Egami, K. Haule, G. Kotliar, and P. Dai, Phys. Rev. Lett. **112**, 217202 (2014).
[33] Q. Si, E. Abrahams, J. Dai, and J.-X. Zhu, New J. Phys. **11**, 045001 (2009).
[34] L. de Medici, S. R. Hassan, M. Capone, and X. Dai, Phys. Rev. Lett. **102**, 126401 (2009).
[35] M. Neupane, P. Richard, Z.-H. Pan, Y.-M. Xu, R. Jin, D. Mandrus, X. Dai, Z. Fang, Z. Wang, and H. Ding, Phys. Rev. Lett. **103**, 097001 (2009).
[36] S. Jiang, L. Liu, M. Schutt, A. M. Hallas, B. Shen, W. Tian, E. Emmanouilidou, A. Shi, G. M. Luke, Y. J. Uemura, R. M. Fernandes, and N. Ni, Phys. Rev. B **93**, 174513 (2016).